Measurement of PAH and soot of diffusion flames in a triple port burner

Kazuhiro Yamamoto[1] and Masahiro Takemoto[2]

Nagoya University, Furo-cho, Chikusa-ku, Nagoya, Aichi 464-8603, Japan

Abstract. Since PAH and soot cause atmospheric pollution, these emissions in practical combustors should be reduced. For that purpose, an approach for precise measurement of PAH and soot concentrations is needed. In this study, we measured PAH and soot of diffusion flames in a triple port burner. The coannular burner consists of three concentric tubes, where air flows in both inner (central) and outer tubes, and fuel flows in the annulus between these air tubes. Two diffusion flames are formed in the boundaries of fuel and air. To detect PAH and soot regions, the techniques of PAH-LIF (laser-induced fluorescence) and soot LII (laser-induced incandescence) were applied. The system of GC/MS was also used to obtain quantitative PAH concentration. Through a comparison of LIF signal and PAH concentrations measured by GC/MS, LIF signals correspond well to the major PAHs of benzene and naphthalene. When the longer excitation wavelength was used, the higher-class PAH was better reflected in LIF signals. For comparison, a diffusion flame in a co-axial burner (simply, double port burner) was examined by changing the fuel and air flow rates. In the triple port burner, the flame height is smaller than that of the double port burner, which could be caused by the promoted mixing of fuel and air. Since PAH which is a precursory substance of soot is decreased in the triple port burner, the total soot in flames is resultantly reduced.

Key words: Diffusion flame, Pollutants, Laser diagnostics, PAH, Soot

Nomenclature

I = signal of soot LII or PAH-LIF
r = radial distance
U_{1A} = internal air flow velocity of triple port burner
U_{2F} = fuel flow velocity of triple port burner
U_{3A} = external air flow velocity of triple port burner
U_A = air flow velocity of double port burner
U_F = fuel flow velocity of double port burner
X_i = mole fraction of species i

z = axial distance
λ = excitation wavelength of laser

1 Introduction

Recent years have witnessed the worsening of environmental problems such as global warming and atmospheric pollution. One of the substances which cause atmospheric pollution is particulate matter including soot, widely emitted from diesel vehicles, combustion furnaces, and other applications [1,2]. Especially, nano-particles are thought to cause asthma and lung cancer, which makes it further desirable to reduce emission amounts. The precursor substances known as polycyclic aromatic hydrocarbons (PAHs) are profoundly related to soot formation [3-6]. New models for PAH and soot have been proposed, captured by a detailed chemical kinetic mechanism [7,8]. Similar to soot, PAH contains many carcinogens [9], making it necessary to reduce the emission amounts of PAH, as well. It is believed that, by measuring PAH and soot following the study of the formation of these substances, will thereby be possible to control their emissions. The emissions of PAH and soot expectedly depend on the design and operating conditions of combustion devices [10]. Thus, as for the reduction of PAH and soot, some fundamental and challenging researches have been reported in many industrial applications including gasoline surrogate fuel [11], biomass combustion [5,12], and coal combustion [13].

So far, we have focused on a triple port burner [14,15]. The burner configuration is quite similar to a coannular burner for inverse diffusion flames [16-18]. The burner has three concentric tubes, where air flows in both inner (central) and outer tubes and fuel flows in the annulus between air tubes (see Fig. 1). Then, there are two boundaries between fuel and air. We have examined the flame structure and combustion characteristics in the triple port burner. Compared with the co-axial burner, the contact area between fuel and air is larger, which enables the promotion of both substances' admixture and reaction. Since the axis of symmetry lies in the oxidizer stream, rather than the fuel stream, the temperature decays more quickly in the fuel rich regions [17], which is confirmed in our simulation [14]. It is expected that PAH and soot formations could be largely reduced.

In this study, both PAH and soot are measured in the triple port burner. In order to discuss the PAH and soot, it is necessary to carry out two-dimensional measurements with high resolution of time and space. Here, a laser-induced fluorescence (LIF) technique is used to measure PAH, while a laser-induced incandescence (LII) technique is used to measure soot [19-25]. These abili-

ties to detect very low concentrations of PAH and soot have been confirmed. Although several experiments have been reported for measuring PAH using LIF, one shortcoming of PAH-LIF is that it is difficult to specify the chemical species of PAH. Then, attempts have been tried to measure species selectively by choosing the laser excitation wavelength and the filter transmission wavelength [26-28].

Here, PAH-LIF measurements at two different excitation wavelengths are tested. Simultaneously, we measure PAH concentrations by means of GC/MS [9,29,30], which enables the identification of chemical species with absolute concentrations, and then compare the results of both sets of measurements. We furthermore vary the flow velocities of supplied fuel and air, thus investigating soot and PAH in flames at different flow conditions. For comparative purposes, we also measure the soot and PAH in the co-axial burner (simply referred to as a " double port burner " in this paper), then revealing the characteristics of the triple port burner.

2 Experimental setup

2.1 Triple port burner

Figure 1 shows a schematic of the triple port burner. Originally, this burner has been developed for the inverse diffusion flame in order to investigate the phenomena in the turbulent buoyant fire plumes where the air is injected into the gaseous fuel by turbulent eddies [16-18]. Due to the unique burner configuration where the fuel is supplied between two air flows, the mixing between fuel and air is promoted [14,15]. The internal air flow nozzle has an inner diameter of 11 mm (rim thickness of 1 mm), the fuel flow nozzle has an inner diameter of 17 mm, the external air flow nozzle has an inner diameter of 57 mm, and mesh, along with glass beads having diameters of 3 mm, are used to regulate both air flows. Propane was used for fuel. In experiments, we used two triple port burners. We refer to this small-model burner in Fig. 1 as " triple port burner (S). " The flow velocity of air flowing in from the center part (internal air flow velocity of U_{1A}) and the fuel flow velocity of U_{2F} were varied. However, the external air flow velocity of U_{3A} was fixed at 19.4 cm/s. As for the coordinate system, r and z represent the radial and axial distances from the center of the burner exit, respectively.

On the other hand, when carrying out GC/MS measurements, a large-model triple port burner (L) was used in order to minimize the influence of sampling probe insertion upon the combustion field. For the triple port burner (L), the internal air flow nozzle has an inner diameter of 74 mm (rim thickness of 1 mm), the internal fuel flow nozzle has an inner diameter of 88 mm, and the external air flow nozzle has an inner diameter of 102 mm. Be-

cause the central air injection port is large, air is supplied through a diffuser, where the flow path is widened and the air flow velocity is subsequently uniform, after which air flow is further regulated by means of glass beads and a two-ply mesh.

For comparison, we constructed the double port burner as reference [31-34]. The fuel nozzle of this double port burner has an inner diameter of 11.1 mm (rim thickness of 1 mm), while the air flow nozzle has an inner diameter of 101.6 mm. The fuel nozzle has the same cross-sectional area as that of the triple port burner (S). The fuel volumetric flow rate being identical for both burners, it is possible to compare the results at the identical fuel supply rate at the same flow velocity. As for the double port burner, we varied the fuel flow velocity (U_F). The air flow velocity was set to be the constant, so that the volumetric flow rate of ambient air was made to be the same as that of external air in the triple port burner (S).

To see the experimental conditions for two burners, flow conditions are shown in Table 1. Typically, the Reynolds number was 350-1490 of internal air flow for triple port burner (S), or 190-1520 of internal air flow for triple port burner (L). In this case, the characteristic length was the diameter of the internal air flow nozzle. The Reynolds number of fuel or external air flow was much smaller. In the present experiments, the flow was almost laminar, and the shear flow caused by the velocity difference between fuel and two air flows was not intense.

Table 1

Burner type	U_{1A}	U_{2F} (U_F)	U_{3A} (U_A)
Triple port burner (S)	9.27, 17.0, 26.9, 39.4 cm/s	2.62 cm/s	19.4 cm/s
Triple port burner (L)	3.9, 19.4, 31.0 cm/s	2.8 cm/s	19.4 cm/s
Doble port burner	-	1.70, 2.62, 4.55 cm/s	5.94 - 19.4 cm/s

2.2   Measurement system

The measurement of PAH concentration was carried out using the LIF method. Figure 2 shows a setup for PAH-LIF system. The beam of a pulsed laser was used to form a thin laser sheet for 2D imaging. A Nd:YAG-pumped dye laser is frequency doubled to 283 nm to excite PAH [17,20]. The laser energy was about 10 mJ/pulse. The fluorescence signal from PAH is generally detectable for only tens of nanoseconds after laser excitation whereas LII signal from soot is detectable for hundreds of nanoseconds. The LII signal typically shows a sharp peak almost coincident with the laser pulse, but has a longer characteristic decay time. The different temporal decay of the emission process allows us to distinguish between LIF and LII signals [1,21]. Then, the same strategy was adopted, coupled with interference filters. In

addition, the third harmonic (wavelength of λ= 355 nm) of the Nd:YAG laser was also used for PAH excitation. The fluorescence from PAH was measured with a gated image-intensified CCD camera (Hamamatsu Photonics C8484). The CCD camera has a resolution of 1024 × 1024 pixels. In this measurement, the laser beam thickness was about 400 μ m, and the resolution of the camera was 23 μ m. The camera lens was equipped with a narrow band-pass filter (FWHM = 10 nm) with the central wavelength at 450 nm [20,34]. The camera gate width was set to be 50 ns. The data deviation in LIF measurement was within 10 %. In order to quantitatively evaluate the PAH fluorescence signal, we used GC/MS (Gas Chromatograph-Mass Spectrometry, Shimadzu, QP5050A) and a sampling probe, with a heated on-line connection between them. Several columns were tested and the CBP middle bore capillary column (Shimadzu, CBP-1, 0.22mm I.D.) was mainly used. As for the sampling line, the pressure drop between the flame and the inlet of the quartz sampling probe was set to ensure rapid quenching of reactions. The transfer line was heated at 553 K. We measured the absolute concentrations of cyclopentadiene, benzene, toluene, phenylacetylene, indene, naphthalene, and phenanthrene. Calibrations were based on direct injection of pure compounds.

On the other hand, the LII technique was used to measure soot volume fraction. For the light source, the second harmonic (wavelength of λ= 532 nm) of the Nd:YAG laser (PRO-R10, manufactured by Spectra Physics) was used [20-25]. A laser sheet was passed through the flame to heat the soot particles up to incandescence temperature [35]. A band-pass filter (FWHM = 10 nm) with the central wavelength at 400 nm was installed in front of ICCD camera [1,20,26]. The image intensifier gate width was 50 ns in order to eliminate light emitted from the flame and background. The data deviation in LII measurement was within 10 % [32]. Although, in our preliminary experiments, it has been confirmed that LII signal is proportional to soot volume fraction [23], any calibrations were not conducted for both LII and LIF signals. In comparing results of two burners, only relative concentrations of soot and PAH were discussed.
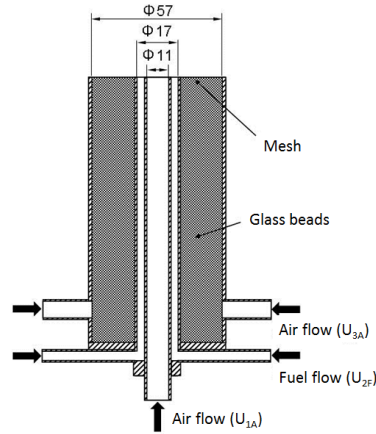
Figure 1: A schematic of triple port burner (S).
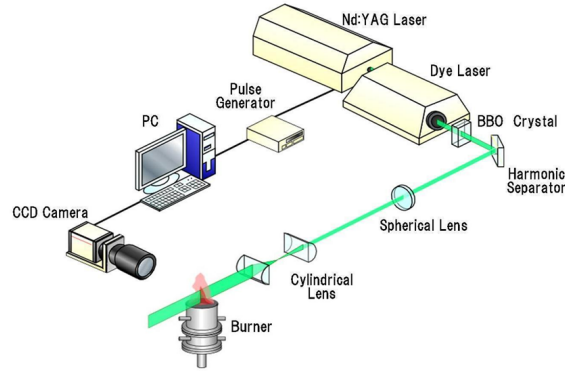
Figure 2: A setup for PAH-LIF system.

3 Results and discussion

3.1 Appearance of flame

Figure 3 shows direct photographs of flames formed by the triple port burner (S). In this case, the fuel flow and external air flow velocities were fixed at U_{2F} = 2.62 cm/s and U_{3A} = 19.4 cm/s, while the internal air flow velocity was varied for U_{1A} = 9.27, 17.0, and 26.9 cm/s. It is seen that, due to the buoyancy effects, the flame largely fluctuates. Clearly shown in this figure, very bright luminous flames are observed for all cases. Although it is not clear that two diffusion flames are merged in downstream, two blue flames are recognized near the burner rims between fuel and air nozzles. Later, the slice image of the luminous flame obtained by LII measurements will be shown.

The flame length is dramatically shorter when the internal air flow velocity is increased. For comparison, photographs of flames using the double port burner are shown in Fig. 4. Fuel flow velocity was varied at U_F = 1.70, 2.62, and 4.55 cm/s, while ambient air flow velocity was fixed at U_A = 5.94 cm/s. Similarly, a luminous flame is observed whereas a blue flame is formed near the burner rim. It is found that the flame length increases when fuel flow velocity is increased. It should be noted that, different from the triple port burner, changes in flame length are small even when ambient air flow velocity is increased to U_A = 19.4 cm/s.

Here, results of both burners are compared at the same fuel flow velocity. Based on Figs. 3 and 4, it is found that, even at the same fuel flow velocity, the flame length of the triple port burner is shorter than that of the double port burner. Interestingly, the flame length can be shorter when more air is supplied from the internal air flow nozzle. This could be explained by the fact that a mixing between fuel and air is promoted in the triple port burner, because air is supplied into the interior of the fuel flow.
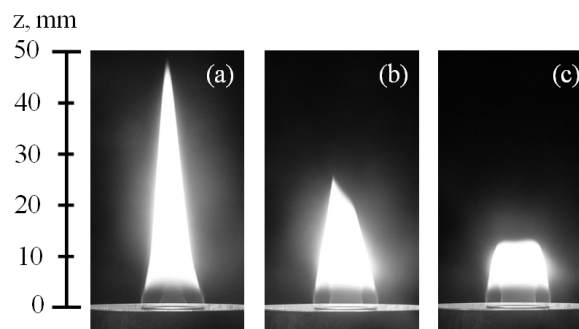
Figure 3: Photographs of flames in the triple port burner (S) for (a) U_{1A} =9.27cm/s,(b) U_{1A} =17.0cm/s, and (c) U_{1A} = 26.9cm/s; U_{2F} = 2.62 cm/s.
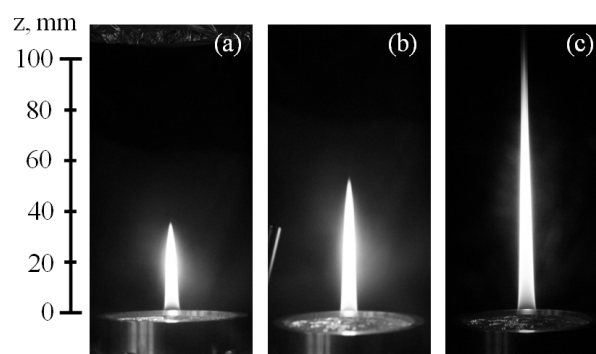
Figure 4: Photographs of flames in the double port burner for (a) U_F =1.70cm/s,(b) U_F =2.62cm/s, and (c) U_F =4.55cm/s.

3.2 PAH measurement

Figure 5 shows PAH-LIF images using the triple port burner (L), which are single-shot fluorescence images. The fuel flow and external air flow velocities were fixed at U_{2F} = 2.8 cm/s and U_{3A} = 19.4 cm/s, while the internal air flow velocity was varied for U_{1A} = 3.9, 19.4, and 31.0 cm/s. For PAH excitation, the laser wavelength of 283 nm was used. Image area was in the range of 28 mm r 52 mm and 8 mm z 32 mm, where the fuel port is located at 38 mm r 44 mm. Based on these images, the PAH regions approximately with 5 mm thickness are well visualized. Also, it is found that there are two separate PAH regions in the upper stream, but they are merged in downstream. This is because two different flames are formed in the triple port burner. Furthermore, increasing the internal air flow velocity causes a slanted LIF distribution to arise. Therefore, increasing U_{1A} causes both flames to incline to one side, which in turn causes variations in PAH regions. Then, a planar laser-induced fluorescence (PLIF) technique is very useful to obtain the slice image of PAH regions with high resolution of time and space.

Figure 6 shows radial distributions of PAH concentration measured by GC/MS. The flow conditions are the same in Fig. 5. In this figure, mole fraction of benzene, naphthalene, and phenanthrene, are shown. Only concentrations of these PAHs were reported, and those of other species were very small in case of triple port burner. Needless to say, it was a point-measurement, and each plot was obtained when the gas at the sampling point was collected and analyzed. The very fine probe (0.3 mm I.D., 0.8 mm O.D.) was used for better spatial resolution. As seen in these profiles, it is found that there are two peaks. The left peak around r = 36-38 mm corresponds to the PAH region in the diffusion flame of internal air and fuel, and the right peak around r = 41-43 mm corresponds to the PAH region in that of fuel and external air. These profiles are similar, and the concentration of benzene is much larger.

Next, we compare these profiles with the PAH-LIF signal. The results are plotted in Fig. 7. To see the relative variation of PAH profiles, the radial PAH profile are normalized by the maximum value. As for the profile of PAH-signal, the averaged profile using 100 fluorescence images is plotted, because the flame fluctuates. Both are obtained at z = 10 mm, which is shown by dotted line in Fig. 5. These profiles are normalized by the maximum values. As seen in this figure, the LIF signal takes on almost exactly the same profile as PAH distributions of benzene and naphthalene measured by GC/MS. In general, the LIF signal may depend on the temperature due to the collision quenching etc., which is confirmed to be less observed in this measurement. In Fig. 6, since concentrations of phenanthrene and other PAHs are much lower than those of benzene and naphthalene. Thus, it is confirmed that the LIF signal corresponds well to these major PAH concentrations, and we can

discuss their emissions based on LIF signals.
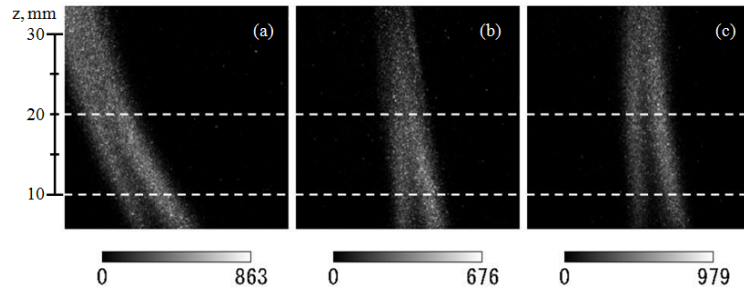
Figure 5: PAH-LIF images of triple port burner (L) for (a) U_{1A} =3.9cm/s, (b) U_{1A} =19.4cm/s, (c) U_{1A} =31.0cm/s.
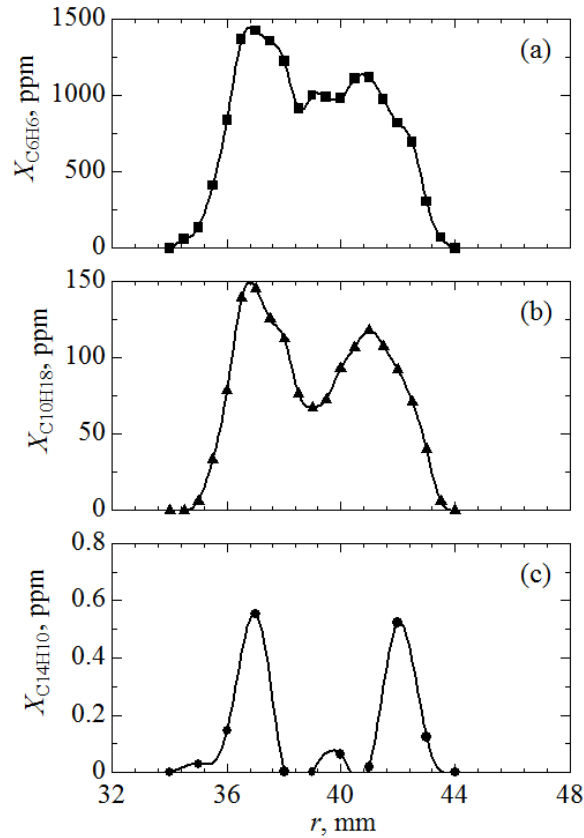
Figure 6: Profiles of PAH-LIF and mole fraction of (a) benzene, (b) naphthalene, and (c) phenanthrene for U_{1A} =19.4 cm/s at z = 10 mm.
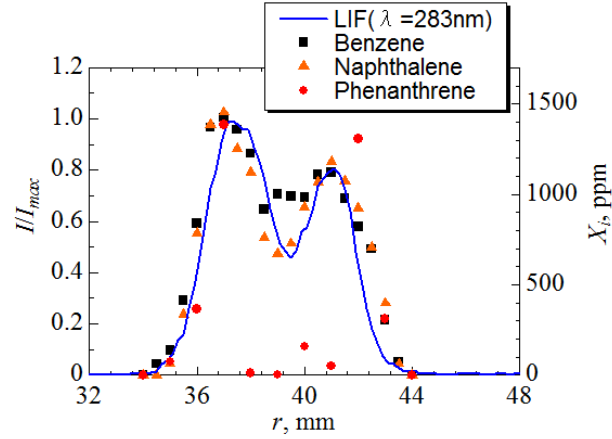
Figure 7: Non-dimensionalized profiles of PAH-LIF and mole fraction of benzene, naphthalene, and phenanthrene for U_{1A} =19.4 cm/s at $z = 10$ mm.

3.3 Soot measurement

Figure 8 shows LII images to see soot regions, which are also single-shot images. The triple port burner (L) was used. The flow conditions and the image area are the same in Fig. 5. Two separate soot regions are observed. To discuss PAH and soot regions, these radial distributions are compared. Since the flame fluctuates, the averaged profiles are obtained using 100 images.

Figure 9 shows the radial distributions of PAH-LIF and LII signals at $z = 20$ mm, which are shown by dotted line in Figs. 5 and 8. In addition, the radial distribution of PAH-LIF signal obtained at the laser excitation wavelength of 355 nm is shown. These profiles are normalized by the maximum values. It is found that PAH region is observed within two soot peaks even when different excitation wavelengths are used. However, by comparing two PAH-LIF distributions, it is found that the distribution at 355 nm is rather shifted toward the soot regions. This could be explained by the fact that PAH is a precursor substance of soot, with PAH forming at an earlier stage than soot particle growth. It has been reported that the higher-class PAH is measured at the greater excitation wavelength [27,28]. In this measurement, it is confirmed that the higher-class PAH is better reflected in signals when the excitation wavelength is 355 nm. Indeed, PAH is detected near the fuel port in Fig. 5 whereas soot is not observed in this region [21].
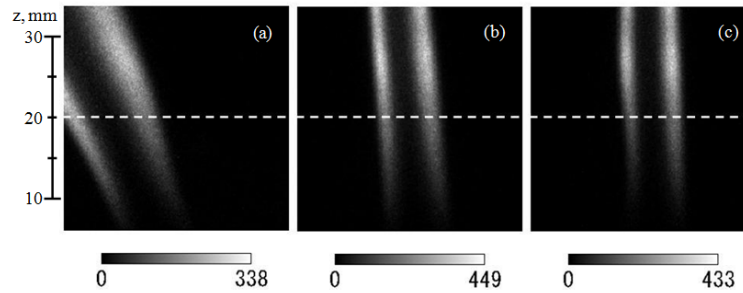
Figure 8: LII images of triple port burner (L) for (a) U_{1A} =3.9cm/s, (b) U_{1A} =19.4cm/s, (c) U_{1A} =31.0cm/s.
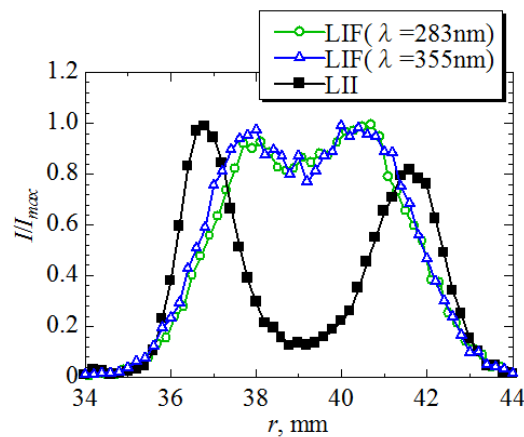
Figure 9: Profiles of PAH-LIF and LII signals of triple port burner (L) for U_{1A} =19.4 cm/s at $z = 20$ mm.

3.4   PAH and soot in flames

To make clear the PAH and soot in flames of the triple port burner, PAH-LIF and LII measurements were conducted using the double port burner. Figures 10 and 11 show PAH-LIF and LII images for both burners, respectively. These are single-shot images. To compare PAH and soot at the same flow conditions, the triple port burner (S) was used. The fuel flow velocity was fixed at $U_F = U_{2F} = 2.62$ cm/s, while the internal air flow velocity in the triple port burner (S) was at $U_{1A} = 9.27$, 17.0, and 26.9 cm/s. The external air flow velocity in the triple port burner (S) was at $U_{3A} = 19.4$ cm/s, while the ambient air flow velocity in the double port burner was at $U_A = 5.94$ cm/s. Image areas were in the range of -20 mm r 20 mm and 0 mm z 70 mm. The laser wavelength of 283 nm was used for PAH-LIF. As before-mentioned, the flame in the double port burner is longer. Since it was not possible to capture the entire flame in one measurement, two images were taken. Due to the

flame fluctuation, the upper image of LII signals in Fig. 11 displays a left-right misalignment at the boundary.

Since two diffusion flames are formed in the triple port burner, two separate PAH and soot regions are formed. However, in downstream, these two regions are merged. As seen in Fig. 10, the peak LIF signal of the triple port burner is much smaller than that of the double port burner, which indicates that PAH formation could be reduced by the triple port burner even at the same fuel and air volumetric flow rates. In Fig. 11, as well, it is found that the maximum soot concentration evaluated by the LII signal of the triple port burner is lower. Therefore, PAH and soot concentrations are simultaneously decreased in the triple port burner.
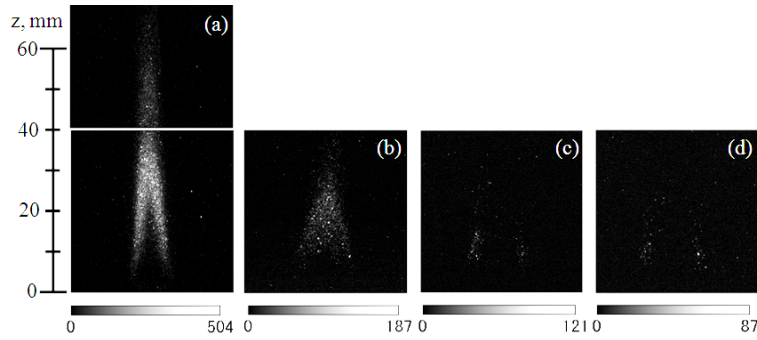
Figure 10: Images of PAH-LIF signal of (a) double port burner, and triple port burner (S) for (b) U_{1A} =9.27cm/s, (c) U_{1A} =17.0cm/s, (d) U_{1A} =26.9cm/s.
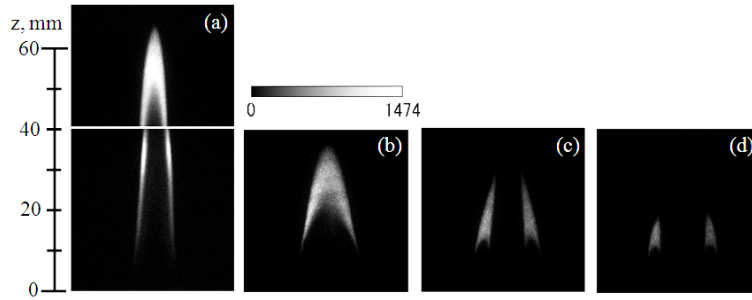
Figure 11: Images of LII signal of (a) double port burner, and triple port burner (S) for (b) U_{1A} =9.27cm/s, (c) U_{1A} =17.0cm/s, (d) U_{1A} =26.9cm/s.

However, in the triple port burner, the flames have large diameters, and two separate flames are formed. There is a possibility that the total amounts of PAH and soot throughout the combustion zone may increase, even when peak PAH and soot concentrations are lower than those in the double port burner. Then, by assuming the axial symmetry, the total PAH and soot in

flames were estimated using the following equation.

$$I_{total} = \int\int_V 2\pi r I(r,z)\,dr\,dz \tag{3.1}$$

where I represents the PAH-LIF or LII signal. Figure 12 shows integrated PAH-LIF signal. Results at different flow conditions are shown, using the triple port burner (S). The internal air flow velocities of U_{1A} are 9.27, 17.0, 26.9, 39.4 cm/s. The fuel flow velocity of U_{2F} and the external air flow velocity of U_{3A} are 2.62 cm/s and 19.4 cm/s, respectively. Averaged values are plotted using 100 images. For comparison, results using the double port burner are plotted. The fuel flow velocity of U_F and air flow velocity of U_A are 2.62 cm/s and 5.94 cm/s. To evaluate the variation of PAH at different flow conditions, the ratio of the fuel volumetric flow rate to the total air volumetric flow rate is calculated, which is the sum of the internal and external air flows. The overall equivalence ratio is also shown. In fact, the total PAH amount is significantly influenced by the changes in equivalence ratio [36].

It is found that the overall equivalence ratio is much lower than unity. That is, within these conditions, the enough air was supplied to oxidize the fuel. At any flow conditions, the total PAH of the triple port burner is much lower. In the triple port burner, as the internal air flow velocity is increased, PAH could be diluted. However, by integrating the PAH-LIF signals, it is found that the total PAH is reduced.

Similarity, the total soot amount in flames for both burners were calculated. Figure 13 shows the integrated LII signals. The flow conditions are the same in Fig.12. It has been reported that the soot formation is affectred by the co-axial air flow in a jet diffusion flame [37]. Expectedly, it is found that the total soot amount of the triple port burner is smaller. Additionally, the soot is further reduced when U_{1A} is increased. Therefore, it is concluded that, in comparison with the double port burner, the mixing between fuel and air is promoted, because air is supplied inside the fuel flow. These are in accordance with the flame height in Figs. 3 and 4. Resultantly, PAH which is a precursory substance of soot is largely reduced, thereby decreasing the soot amount. These results could be very useful to reduce pollutants including PAH and soot by enhancing the mixing of fuel and air. In future, based on the simulation results [14,15], we will see the flow field and local equivalence ratio to discuss the effect of mixing on PAH and soot formations.
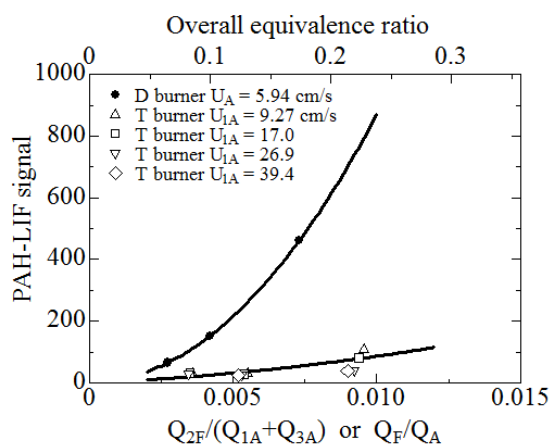
Figure 12: Integrated LIF signals for total PAH emission at different flow conditions are shown. To evaluate the variation of PAH emission at different flow conditions, the ratio of the fuel volume rate to the total air volume rate is calculated.
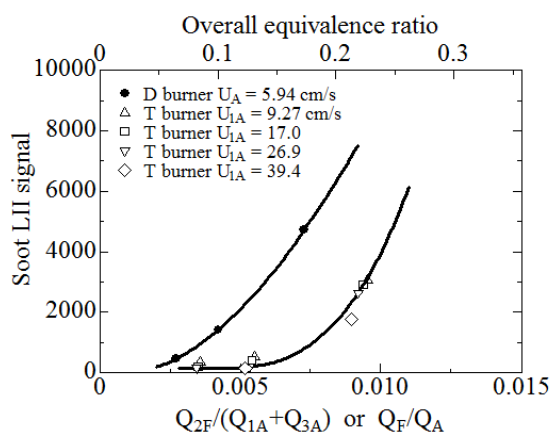
Figure 13: Integrated LII signal for total soot emission at different fuel flow velocity is shown. Flow conditions are the same in Fig.12.

4 Conclusions

In this study, by using PAH-LIF and LII, we evaluated PAH and soot in flames of the triple port burner. Two different excitation wavelengths were tested. Simultaneously, we measured PAH concentrations by GC/MS. The fuel flow and air flow velocities were changed. For comparative purposes, we also measured the soot and PAH in the co-axial burner (double port burner),

and then revealed the characteristics of the triple port burner. The following conclusions were obtained.

(1) In PAH measurements, there are two peaks in the radial profiles. One corresponds to the PAH region of internal air and fuel, and the other corresponds to that of fuel and external air. Through a comparison of LIF signal and PAH concentration measured by GC/MS, LIF signal matches the major PAH concentrations of benzene and naphthalene. When the longer excitation wavelength is used, the higher-class PAH is better reflected in LIF signals.

(2) Since two diffusion flames are formed in the triple port burner, two separate PAH and soot regions are observed. However, in downstream, these two regions are merged. When radial distributions of PAH and soot are compared, there are two peaks in soot regions, with maximum PAH concentration existing between them. This could be explained by the fact that PAH is a precursor substance of soot, with PAH forming at an earlier stage than soot particle growth. Indeed, only PAH is detected near fuel port.

(3) When PAH and soot concentrations of both burners are compared by keeping the same fuel and air volumetric flow rates, these maximum values are greatly decreased in the triple port burner. By integrating PAH-LIF and LII signals, it is found that total PAH and soot in flames are reduced. In the triple port burner, when the internal air flow velocity is increased, the mixing between fuel and air is further promoted, causing the flame length to be shortened with lower PAH and soot amounts.

References

[1] R.L. Vander Wal, K.A. Jensen, M.Y. Choi, Simultaneous laser-induced emission of soot and polycyclic aromatic hydrocarbons within a gas-jet diffusion flame, Combust. Flame 109 (1997) 399-414.
[2] A. D'Anna, Combustion-formed nanoparticles, Proc. Combust. Inst. 32 (2009) 593-613.
[3] O.S.L. Bruinsma, J.A. Moulijn, The pyrolytic formation of polycyclic aromatic hydrocarbons from benzene, toluene, ethylbenze, styrene, phenylacetylene and n-decane in relation to fossil fuels utilization, Fuel Proc. Technol., 18 (1988) 213-236.
[4] N. Olten, S. Senkan, Formation of polycyclic aromatic hydrocarbons in an atmospheric pressure ethylene diffusion flame, Combust. Flame 118 (1999) 500-507.
[5] A.A. Khan, W. de Jong, P.J. Jansens, H. Spliethoff, Biomass combustion in fluidized bed boilers: Potential problems and remedies, Fuel Proc. Technol., 90 (2009) 21-50.
[6] A. Faccinetto, P. Desgroux, M. Ziskind, E. Therssen, C. Focsa, High-sensitivity detection of polycyclic aromatic hydrocarbons adsorbed onto soot particles using laser desorption/laser ionization/time-of-flight mass spectrometry: An approach to studying the soot inception process in low-pressure flames, Combust. Flame, 158 (2011) 227-239.

[7] M. Sander, R.I.A. Patterson, A. Braumann, A. Raj, M. Kraft, Developing the PAH-PP soot particle model using process informatics and uncertainty propagation, Proc. Combust. Inst. 33 (2011) 675-683.

[8] T. Blacha, M. Di Domenico, P. Gerlinger, M. Aigner, Soot predictions in premixed and non-premixed laminar flames using a sectional approach for PAHs and soot, Combust. Flame, 159 (2012) 181-193.

[9] M.S. Callen, M.T. de la Cruz, J.M. Lopez, A.M. Mastral, PAH in airborne particulate matter.: Carcinogenic character of PM10 samples and assessment of the energy generation impact, Fuel Proc. Technol., 92 (2011) 176-182.

[10] M.K. Bobba, M.P.B. Musculus, Laser diagnostics of soot precursors in a heavy-duty diesel engine at low-temperature combustion conditions, Combust. Flame, 159 (2012) 832-843.

[11] B.C. Choi, S.K. Choi, S.H. Chung, Soot formation characteristics of gasoline surrogate fuels in counterflow diffusion flames, Proc. Combust. Inst. 33 (2011) 609-616.

[12] B.M Jenkins, L.L Baxter, T.R Miles Jr., T.R Miles, Combustion properties of biomass, Fuel Proc. Technol., 54 (1998) 17-46.

[13] Y. Ninomiya, L. Zhang, A. Sato, Z. Dong, Influence of coal particle size on particulate matter emission and its chemical species produced during coal combustion, Fuel Proc. Technol., 85 (2004) 1065-1088.

[14] G. Okuyama, K. Yamamoto, N. Hayashi, H. Yamashita, Combustion characteristics and flame structure in a triple port burner, Proc. 6th Int. Conf. Computational Heat and Mass Transfer (2009) 373-378.

[15] K. Yamamoto, S. Kato, Y. Isobe, N. Hayashi, H. Yamashita, Lifted flame structure of coannular jet flames in a triple port burner, Proc. Combust. Inst. 33 (2011) 1195-1201.

[16] L.G. Blevins, R.A. Fletcher, B.A., Benner Jr., E.B. Steel, G.W. Mulholland, The existence of young soot in the exhaust of inverse diffusion flames, Proc. Combust. Inst. 29 (2002) 2325-2333.

[17] C.R. Shaddix, T.C. Williams, L.G. Blevins, R.W. Schefer, Flame structure of steady and pulsed sooting inverse jet diffusion flames, Proc. Combust. Inst. 30 (2005) 1501-1508.

[18] M.A. Mikofski, T.C. Williams, C.R. Shaddix, L.G. Blevins, Flame height measurement of laminar inverse diffusion flames, Combust. Flame 146 (2006) 63-72.

[19] Y. Xin, J.P. Gore, Two-dimensional soot distributions in buoyant turbulent fires, Proc. Combust. Inst. 30 (2005) 719-726.

[20] S.S. Yoon, S.M. Lee, S.H. Chung, Effect of mixing methane, ethane, propane, and propene on the synergistic effect of PAH and soot formation in ethylene-base counterflow diffusion flames, Proc. Combust. Inst. 30 (2005) 1417-1424.

[21] A. D'Anna, M. Commodo, S. Violi, C. Allouis, J. Kent, Nano organic carbon and soot in turbulent non-premixed ethylene flames, Proc. Combust. Inst. 31 (2007) 621-629.

[22] Y. Bouvier, C. Mihesan, M. Ziskind, E. Therssen, C. Focsa, J.F. Pauwels, P. Desgroux, Molecular species adsorbed on soot particles issued from low sooting methane and acetylene laminar flames: A laser-based experiment, Proc. Combust. Inst. 31 (2007) 841-849.

[23] K. Yamamoto, F. Fujikake, Y. Taya, N. Hayashi, H. Yamashita, S. Gakei, Soot measurement and application on diesel exhaust gas using laser-induced incandescence, Transactions of the Japan Society of Mechanical Engineers, Series B, 74(738) (2008) 498-504.

[24] F. Goulay, P.E. Schrader, L. Nemes, M.A. Dansson, H.A. Michelsen, Photochemical interferences for laser-induced incandescence of flame-generated soot, Proc. Combust. Inst. 32 (2009) 963-970.

[25] R. Lemaire, A. Faccinetto, E. Therssen, M. Ziskind, C. Focsa, P. Desgroux, Experimental

comparison of soot formation in turbulent flames of diesel and surrogate diesel fuels, Proc. Combust. Inst. 32 (2009) 737-744.

[26] S.M. Lee, S.S. Yoon, S.H. Chung, Synergistic effect on soot formation in counterflow diffusion flames of ethylene-propane mixtures with benzene addition, Combust. Flame 136 (2004) 493-500.

[27] F. Beretta, A. D'Alessio, A. D'Orsi, P. Minutolo, U.V. and visible laser excited fluorescence from rich premixed and diffusion flames, Combust. Sci. Tech. 85(1-6) (1992) 455-470.

[28] T. Aizawa, H. Kosaka, Y. Matsui, Measurements of excitation-emission matrix of PAHs in a flame using a multi-wavelength laser source, Transactions of the Japan Society of Mechanical Engineers, Series B 70(690) (2004) 496-502.

[29] M.S. Callen, M.T. de la Cruz, S. Marinov, R. Murillo, M. Stefanova, A.M. Mastral, Flue gas cleaning in power stations by using electron beam technology. Influence on PAH emissions, Fuel Proc. Technol., 88 (2007) 251-258.

[30] E. Pousse, Z.Y. Tian, P.A. Glaude, R. Fournet, F. Battin-Leclerc, A lean methane premixed laminar flame doped with components of diesel fuel part III: Indane and comparison between n-butylbenzene, n-propylcyclohexane and indane, Combust. Flame, 157 (2010) 1236-1260.

[31] T.K.C. Smyth, J.E. Harrington, E.L. Johnson, M.W. Pitts, Greatly enhanced soot scattering in flickering CH4/air diffusion flames, Combust. Flame 95 (1993) 229-239.

[32] C.R. Kaplan, C.R. Shaddix, K.C. Smyth, Computations of enhanced soot production in time-varying CH4/air diffusion flames, Combust. Flame, 106 (1996) 392-405.

[33] C.R. Shaddix, K.C. Smyth, Laser-induced incandescence measurements of soot production in steady and flickering methane, propane, and ethylene diffusion flames, Combust. Flame, 107 (1996) 418-452.

[34] K.C. Smyth, C.R. Shaddix, D.A. Everest, Aspects of soot dynamics as revealed by measurements of broadband fluorescence and flame luminosity in flickering diffusion flames, Combust. Flame, 111 (1997) 185-207.

[35] C.J. Dasch, Continuous-wave probe laser investigation of laser vaporization of small soot particles in a flame, Applied Optics, 23 (1984) 2209-2215.

[36] F. Inal, Artificial neural network predictions of polycyclic aromatic hydrocarbon formation in premixed n-heptane flames, Fuel Proc. Technol., 87 (2006) 1031-1036.

[37] B.H. Jeon, O. Fujita, Y. Nakamura, H. Ito, Effect of co-axial flow velocity on soot formation in a laminar jet diffusion flame under microgravity, J. Thermal Sci. Tech., 2(2) (2007) 281-290.